# 5 A Large, Flux-Limited Sample of Carbon Stars

## 5.1 Introduction

Since carbon can reach the surface of an isolated star only in late evolutionary states, it has long been assumed that all carbon stars are *giants*. Due to their high luminosity it is possible to detect them at large distances: Brewer et al. (1996) have identified C stars even in the local group galaxy M31. As members of our own Galaxy, they are useful as tracers for the kinematics of the halo (e.g., Mould et al. 1985; Morrison et al. 2000), and as "test particles" for weighing the Galactic potential well. For these purposes, faint high galactic latitude carbon (FHLC) stars have been searched by objective prism surveys (e.g., Sanduleak & Pesch 1988; MacAlpine & Lewis 1978) and in the CCD survey of Green et al. (1994).

However, there was one exception known for a long time. Trigonometric parallax measurements for the carbon star G77-61 showed that this star, having $M_V = +9.6$ (Dahn et al. 1977), lies close to the main sequence. Another dwarf carbon star (dC), KA 2, was discovered in the 1980s by Ratnatunga (1983) in the course of an objective prism survey, and was proven to be a dwarf by its high proper motion (p.m.). In the early 1990s, a real "inflation" of dC discoveries took place: Green et al. (1991, 1992) discovered 4 further dCs, again due to their high p.m. Warren et al. (1993) list another 3 possible dCs, but however, the p.m. measurement of only one of them has a significance $> 3\sigma$. Heber et al. (1993) reported that PG 0824+289, a hot DA white dwarf, is in a double-line spectroscopic binary with a dC companion of absolute magnitude very similar to G77–61 ($M_V \sim +10$). Another DA/dC composite system, CBS 311, was discovered by Liebert et al. (1994). Margon et al. (1999) recently reported the discovery of one certain, and one likely dC in the commissioning data of the Sloan Digitized Sky Survey (SDSS).

From its radial velocity variation, G77-61 is known to be a binary; Dearborn et al. (1986) report a period of 245 days. This means that three dCs (the other two being PG 0824+289 and CBS 311) out of $\sim 10$ dCs are *known* to be members of binary systems. Therefore, the most reasonable explanation of the prominent carbon bands in these dwarf spectra is mass transfer from a companion during the companion's second ascent of the giant branch. The enhanced Barium abundance and the wide range of Carbon isotope ratios observed in 6 dCs by Green & Margon (1994) support this scenario.

With about 10 dC stars now known from an incomplete hodgepodge of surveys and serendipity, the conclusion seems inescapable that many more C giants than C dwarfs are presently known only by virtue of the much greater luminosities of the former class. From a p.m. survey of 39 FHLC stars, Green et al. (1992) concluded that the local space density of dCs probably surpasses that of all other types of C stars combined. They found 5 stars (or 13 %) out of their sample to be dwarfs. Assuming $M_V = +10$ for dwarfs, an average of $M_V = +1$ for all other C stars, and assuming that the sample is flux-limited, this would mean that the space density of dCs is $\sim 37\,000$ times higher than the space density of all other C stars! This conclusion is *conservative*, since disk dCs may remain in the FHLC star sample, with p.m.s below the detection threshold. Thus, contrary to the formerly prevailing paradigm, dwarf C stars are likely to be the numerically dominant type of carbon star in the Galaxy.

The discovery of so many dCs, and the remarkable similarity of their spectra to those of C giants means that care must be taken to distinguish dwarfs from giants in FHLC star samples intended for dynamics (Green et al. 1992). As innocent bystanders in a mass transfer binary (MTB) system, dC's spectroscopic and orbital properties provide valuable fossil records of the history and evolution of an extinct population of AGB stars. Even using conservative constraints on the shape of the initial mass function and binary fractions in the disk and spheroid, we may expect mass transfer to have occurred in a large number of such systems (de Kool & Green 1995). The majority of these low mass, post MTB

stars could be M dwarfs, in which the evidence for past mass transfer may be subtle, or even undetectable. In dCs, the spectroscopic signature of extensive mass transfer is glaringly obvious. However, not all dCs have detectable p.m.s, so other luminosity/distance indicators are needed. Comparison of high resolution optical spectra to model atmospheres might seem promising, but most dCs have $V \geq 15$, and thus spectroscopy of sufficient resolution for luminosity estimates is difficult. Green et al. (1992) have shown that high p.m. FHLC stars may exhibit distinctive *JHK* colors appropriate to late-type dwarfs, suggesting infrared colors as a possible luminosity indicator. However, the sample of known dCs is still too small to draw any definitive conclusions.

Larger samples of all types of FHLC stars are thus of interest: giants as tracers of outer halo dynamics and structure (as can be seen in Fig. 31, C stars with distances of up to $\sim 30$ kpc can be found in the HES), and dC stars in particular to improve our fledging understanding of their evolution, and to investigate possible luminosity indicators other than p.m. We are therefore undertaking a two-part investigation. We select C stars in the HES with automated selection techniques, to compile a large, uniformly selected, and flux-limited sample of FHLC stars. We complement this sample with recent epoch CCD astrometry, to measure p.m.s for as many objects as possible, and thereby separate the dCs from C giants.

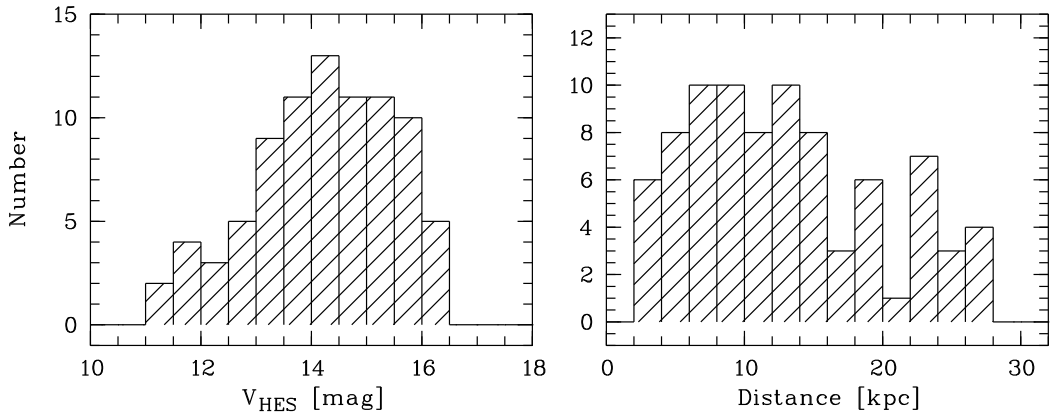


Figure 31: Magnitude and distance distribution of 86 HES carbon stars without significant p.m. $V$ has been derived from the HES spectrum, using Eq. 1 for conversion between $B_J$ and $B$, and the $B-V$ calibration of `dx_hpp2` for red stars given in Tab. 6. Rough distances have been derived by assuming $M_V = -1.0$.

## 5.2 Carbon Star Selection

Carbon stars can be identified in the HES with high confidence without follow-up slit spectroscopy, based on their strong $C_2$ and CN bands. A representative collection of HES spectra of C stars is shown in Fig. 37. Most importantly, C stars can be distinguished from other late type stars, e.g. M or S stars, even if only weak C bands are present in their spectra (see Fig. 32).

Moreover, C stars can be distinguished reliably from white dwarfs of type DQ (hereafter shortly referred to as DQs), since the latter usually have a much bluer continuum (see Fig. 37). The average $U-B$ of HES C stars is $\sim 0.9$, more than 90 % have $U-B > 0.5$, and there is *no* C star of $U-B < 0$ in the HES sample. McCook & Sion (1999) list 49 DQs, of which 30 have an available $U-B$ measurement. The average $U-B$ of those is $-0.58$, i.e., $\sim 1.5^{\rm m}$ away from the average $U-B$ of the HES C star sample. However, 4 objects (i.e., 13 % of the 30 objects with available $U-B$) have $U-B > 0.0$.

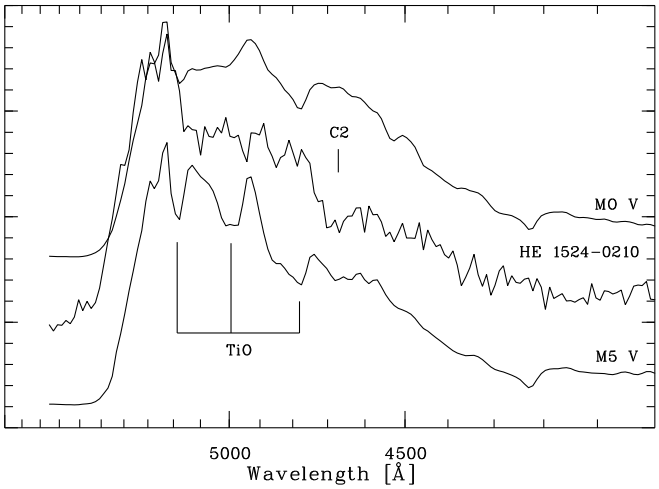


Figure 32: Comparison of HES spectra of the C star HE 1524−0210, exhibiting a weak C band only, with two M stars. The abscissa is density in arbitrary units.

With a rough estimate of the surface density we can quantify by how many "red" ($U-B>0.0$) DQs the HES C star sample is expected to be contaminated. First of all, we have to take into account that the ratio of northern hemisphere to southern hemisphere DQs is unbalanced in McCook & Sion (1999), as much as the *total* catalog is. This is because the southern hemisphere so far has been surveyed less extensively for white dwarfs. Assuming that the northern hemisphere sample of DQs is complete, we derive a surface density of 9 DQs brighter than $V=16.5$ in 20 000 deg$^2$, i.e. $4.5\cdot10^{-4}$ deg$^{-2}$. Hence, the surface density of $U-B>0.0$ DQs is $5.9\cdot10^{-5}$ deg$^{-2}$, and we expect 0.45 DQs to be present on all 380 HES plates (effective area 7 700 deg$^2$). Even if we assume that the sample of DQs known so far is by a factor of 2 incomplete, we statistically expect less than 1 DQ to be present in the final HES C star sample.

We select carbon star candidates in the HES by two methods: A carbon band index method (Sect. 5.2.1), and template matching (Sect. 5.2.2). We inspect all automatically selected spectra individually to identify any remaining plate artifacts, to reject the few overlapping spectra that have not been recognized by the automatic overlap detection procedure (see p. 9), and to verify their C star nature.

### 5.2.1 C Band Index Method

In the carbon band index method, we select stars when the mean $S/N$ in the relevant wavelength range is $>5$ per pixel and both of the $C_2$ bands λλ5165, 4737, or both of the CN bands λλ4216, 3883 are stronger than a selection threshold. Band strengths are measured by means of line indices – ratios of the mean photographic densities in the carbon molecular absorption features and the continuum bandpasses shown in Fig. 33, and listed in Tab. 10. The use of *pairs* of indices prevents confusion with plate artifacts, e.g., scratches. It is very unlikely that two such artifacts are present at the positions of two molecular bands. Selection boxes in the $I\,(C_2\,\lambda5165)$ versus $I\,(C_2\,\lambda4737)$ and $I\,(CN\,\lambda4216)$ versus $I\,(CN\,\lambda3883)$ planes have been chosen well-separated from the dense locus of "normal" stars (see Fig. 34).

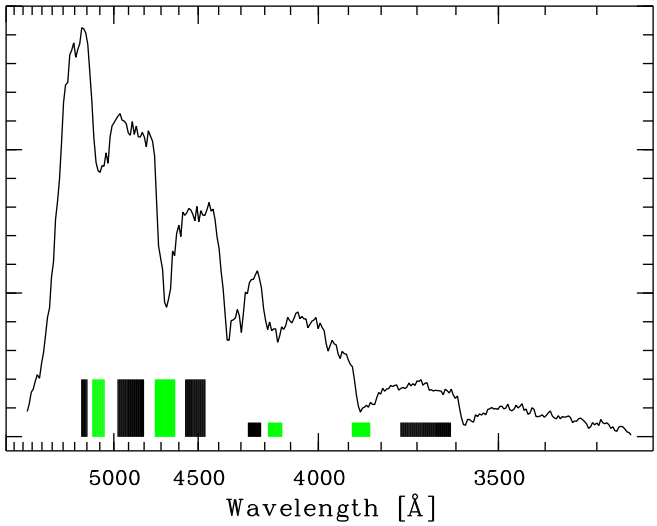


Figure 33: HES objective prism spectrum of the R-type carbon star CGCS 2954 (Stephenson 1989), illustrating the positions of continuum (black) and band (grey) bandpasses defining the $C_2$ (high boxes) and CN (flat boxes) line indices. The abscissa is density in arbitrary units.

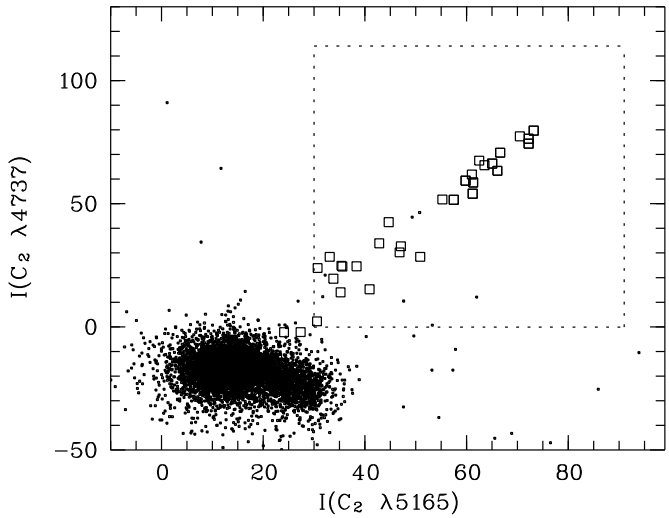


Figure 34: Selection of carbon stars in the $I\,(\mathrm{C}_2\,\lambda 5165)$ versus $I\,(\mathrm{C}_2\,\lambda 4737)$ plane. Band strengths are measured by line indices in arbitrary units. '·' – all spectra on a randomly chosen HES plate, '□' – test sample of known FHLC stars present on HES plates (see Tab. 12), dashed box – selection region. Spectra in which only *one* high $C_2$ band index value has been measured suffer either from an overlapping spectrum, or from a plate artifact. The selection in the $I\,(\mathrm{CN}\,\lambda 4216)$ versus $I\,(\mathrm{CN}\,\lambda 3883)$ plane is done analogously. The two test sample objects outside the selection box are CGCS 525 and CGCS 3180. They are selected by CN band indices (see Tab. 12).

| Passband | Use for band index | | | |
|---|---|---|---|---|
| | $C_2$ 5165 | $C_2$ 4737 | CN 4216 | CN 3883 |
| 5190–5240 Å | cont | | | |
| 5060–5150 Å | flux | | | |
| 4800–4970 Å | cont | cont | | |
| 4620–4730 Å | | flux | | |
| 4460–4560 Å | | cont | | |
| 4210–4270 Å | | | cont | |
| 4130–4180 Å | | | flux | |
| 3830–3890 Å | | | | flux |
| 3610–3740 Å | | | | cont |

Table 10: Wavelengths of C band passbands used for computation of band indices.

### 5.2.2 Template Matching

In the HES, some care must be taken when objects with p.m. shall be selected. This is because the input catalog for extraction of objective prism spectra is generated by using the Digitized Sky Survey I (DSS I). Therefore, large proper motions and/or large epoch differences between HES and DSS I plates (13.5 years on average, see Fig. 35) may result in non-detection of objects in the HES (if $\mu_\alpha \cdot \Delta t_{\text{HES-DSS I}} \gtrsim 4''$, i.e., $> 3$ pixels), and/or an offset of the wavelength calibration zero point, resulting in wrong C band measurements. Therefore, we use a template matching algorithm (see e.g. Castleman 1979, for the concept of template matching), which compensates for offsets in dispersion direction by *shifting* the templates through each spectrum.

As is shown in Fig. 36, p.m.s of a typical halo object ($<u>=<w>= 0$ km/s; $<v>\sim 200$ km/s) result mainly in offsets along declination (i.e., parallel to the HES dispersion direction), and only small offsets in R.A.

We have generated 7 carbon star templates by using a wide range of carbon star types (see Fig. 37). For these spectra a (pseudo-)continuum is determined by median filtering, and subsequent smoothing with a narrow Gaussian filter. These templates are shifted in the range $-20\ldots+20$ pixels in sub-pixel steps along the dispersion direction of (again continuum divided) HES spectra. The shift range corresponds to $\pm 27''$.

For each shift step $j$, realized by template offsets, the template scaling factor $c_j$ is computed by means of a least squares fit, i.e.,

$$\chi_j^2 = \sum_{i=1}^{n_j} \frac{(s_i - c_j \cdot t_{i-j})^2}{\sigma_i^2} \stackrel{!}{=} \min. \tag{25}$$

$s_i$ are the pixels of the spectrum, and $t_i$ the template pixels; $\sigma_i$ is the pixel-wise noise. The sum runs over all $n$ pixels for which the shifted template is defined. The amplitude of the pixel-wise noise as a function of density $D$ is determined plate-wise using an absorption line free spectral region of A-type stars (Sect. 2.2.6; see also Christlieb 1995). Minimizing the $\chi^2$ sums for each shift step yields template scaling factors $c_j$,

$$c_j = \frac{\sum_{i=1}^{n_j} \frac{s_i \cdot t_{i-j}}{\sigma_i^2}}{\sum_{i=1}^{n_j} \frac{t_{i-j}^2}{\sigma_i^2}}. \tag{26}$$

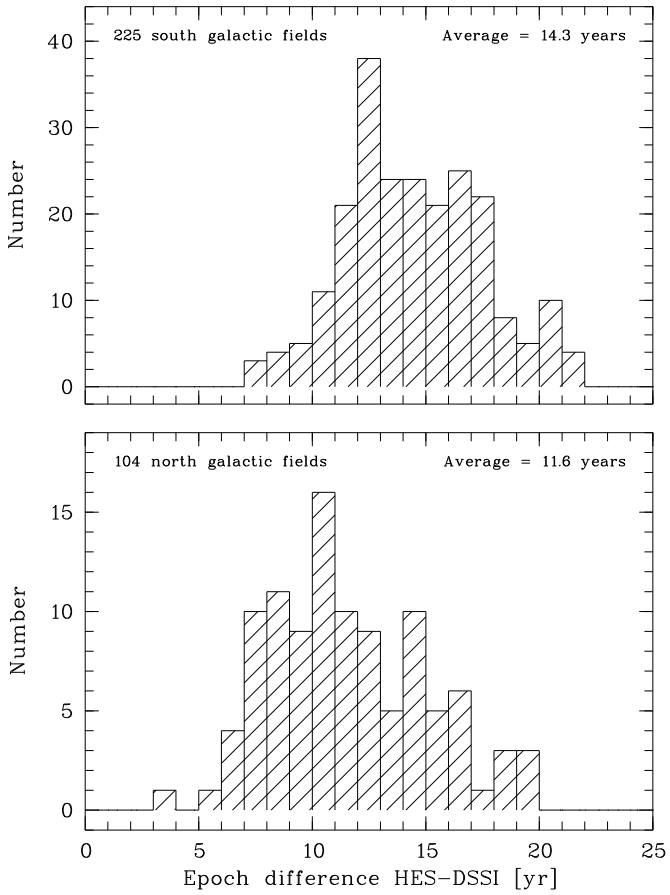


Figure 35: Histograms of epoch differences $\Delta t$ between HES plates and DSS I plates used for spectral reduction. $\Delta t$ is 2.7 yr less on average for the 104 HES plates of north Galactic fields. The total average for all 329 plates is 13.5 yr.

We adopt the template scaling factor $c_j$, which has the lowest $\chi^2$ probability $P(\chi_j^2|\nu_j)$. That is, we look for the offset at which the template "matches best". $\nu_j$ is the number of degrees of freedom, i.e. $\nu_j = n_j - 1$.

Cutoff template scaling factors $c_{\min}$ are determined plate-wise, and for each template, by computing average template scaling factors $\overline{c}$, and standard deviations $\sigma_c$. We use a $5\sigma$ cutoff, i.e.

$$c_{\min} = \overline{c} + 5\sigma_c. \tag{27}$$

A spectrum is selected as C star candidate, if the template scaling factor for *at least one* template is above the cutoff. Note that template matching is not carried out for HES spectra above the saturation threshold, because we do not have an estimation of pixel-wise noise for these.

## 5.3 Testing the Automatic Selection

We tested the automatic selection extensively, and by various methods. In Sect. 5.3.1, we investigate the selection probability as a function of $\mu_\delta \Delta t$ for both selection algorithms. In Sect. 5.3.2 we derive the plate-wise selection probability for halo dCs on HES plates. The results of tests with "real" objects are given in Sect. 5.3.3, and in Sect. 5.3.4 we investigate the selection efficiency.

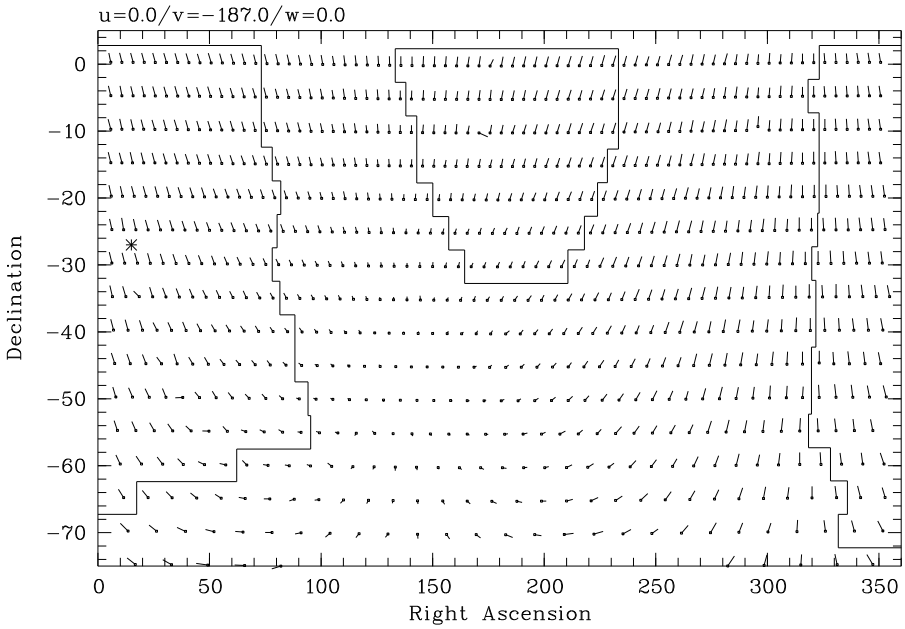


Figure 36: Simulation of p.m. directions.

### 5.3.1 Dependence of Selection Probability on $\mu_\delta \Delta t$

As a test sample for our investigation of the dependence of the selection probability on $\mu_\delta \Delta t$, we used a sample of 78 C stars from HES 44 plates *without* significant p.m. (as measured in the follow-up campaign '99 April at the ESO 2.2 m; see Sect. 5.5), below saturation threshold, i.e. object classes `stars` and `ext`. These were shifted in 1 pixel ($= 1\farcs35$) steps through the range $-700\,\mu\mathrm{m} < x < +700\,\mu\mathrm{m}$, corresponding to $-47\farcs25 < \mu_\delta \Delta t < 47\farcs25$. At each shift step, both selection algorithms have been applied.

The result is displayed in Fig. 38. The combined relative selection rate of both selection methods is $> 50\,\%$ for $-4\farcs5 < \mu_\delta \Delta t < 2\farcs5$. At larger $\mu_\delta t$, the selection rate is nonzero only for the selection by template matching, with exception of two regions with very high $|\mu_\delta \Delta t|$ (where it is unlikely to find a star in reality). The peak selection rate for template matching, around $\mu_\delta \Delta t = 0$, is hardly above 50 %, and is $\sim 30\,\%$ at larger $|\mu_\delta \Delta t|$. Since the test sample has originally been selected by the C band index method, the peak selection rate for this method obviously *has* to be 100 %.

### 5.3.2 Decrease of Selection Probability for Halo dCs

In order to estimate how many dCs are expected to be missed in our survey due to the epoch difference problem, we carried out a simulation study in which the plate-wise selection function for halo dCs was determined. The simulation is similar to that described in Green et al. (1992). We let some dwarfs "fly through space" with halo kinematics, as given by Norris (1986). For the solar neighborhood, he gives

$$v_{\mathrm{rot}} = 37 \pm 10\,\mathrm{km/s} \Longleftrightarrow <v> = -187\,\mathrm{km/s}, \tag{28}$$

and he determined the velocity ellipsoid to be

$$\sigma_u = 131 \pm 6\,\mathrm{km/s} \tag{29}$$

$$\sigma_v = 106 \pm 6\,\mathrm{km/s} \tag{30}$$

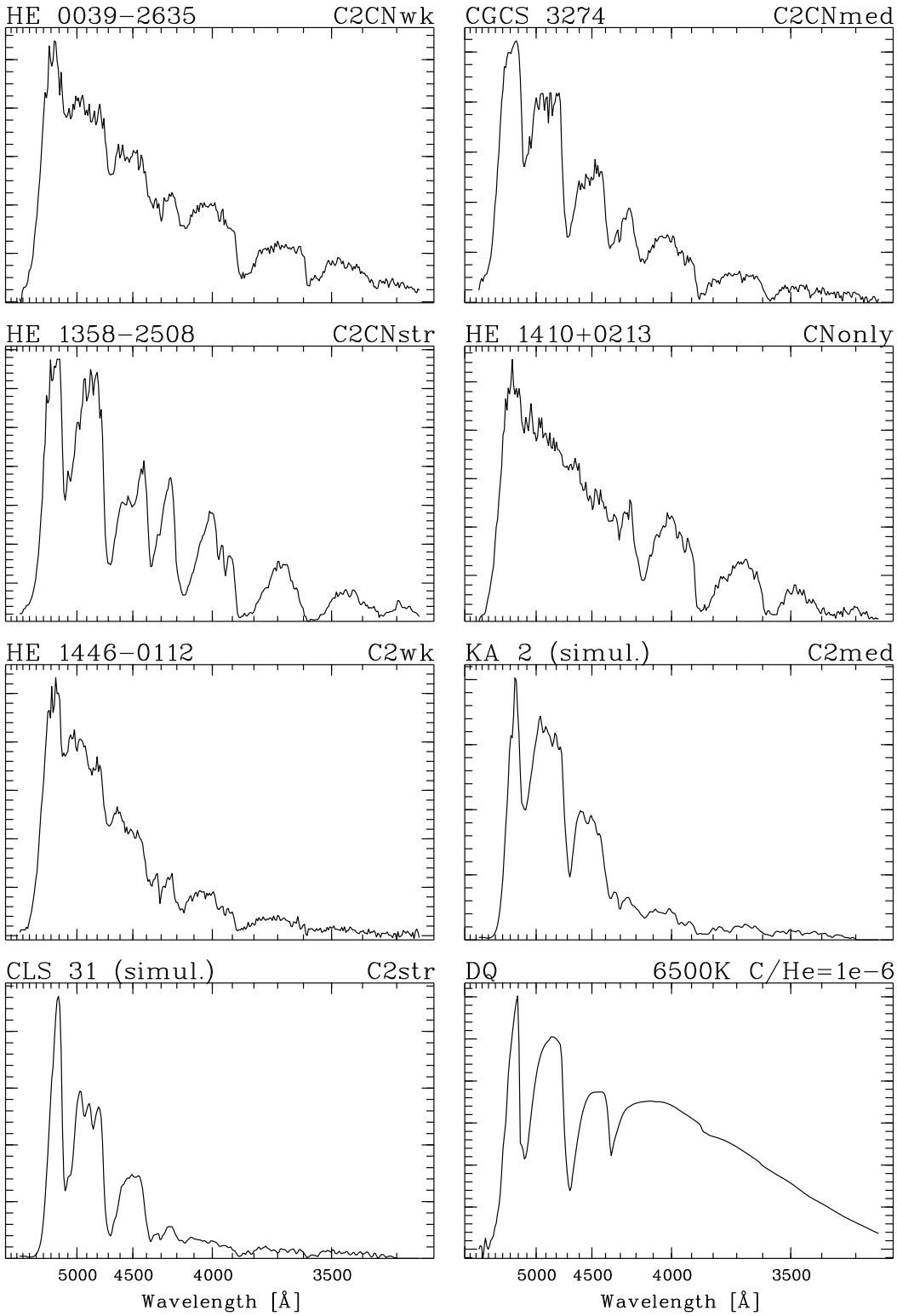


Figure 37: Objective prism spectra of seven C stars used as templates. The spectra of KA 2 and CLS 31 have been derived from slit spectra using the procedures described in Sect. 3.1 on p. 17ff. For comparison, the spectrum of a DQ white dwarf with $T_{\rm eff} = 6\,500\,\mathrm{K}$ and $\mathrm{C/He} = 10^{-6}$ is shown in the lower right panel. That star has $U - B = -0.6$.

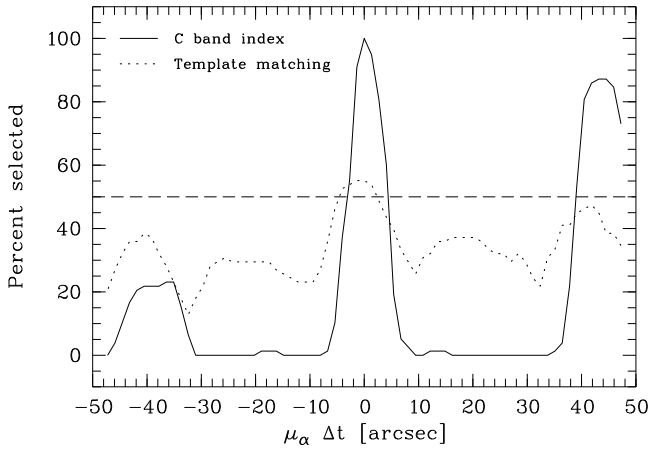


Figure 38: C star selection function in dependence of simulated proper motion $\mu_\alpha \cdot \Delta t$, for template C band index method (solid line), and template matching (dotted line). Selection by template matching has a higher effectivity in the ranges $-30'' \lesssim \mu_\alpha \Delta t \lesssim -2''$ and $5'' \lesssim \mu_\alpha \Delta t \lesssim 40''$.

$$\sigma_w \quad = \quad 85 \pm 6\,\mathrm{km/s}. \tag{31}$$

In each simulation we constructed 100 random velocity vectors $(u,v,w)$, with components following Gaussian distributions according to the above parameters, i.e.

$$\begin{pmatrix} u \\ v \\ w \end{pmatrix} = \begin{pmatrix} N(\quad 0\,\mathrm{km/s}, 131\,\mathrm{km/s}) \\ N(-187\,\mathrm{km/s}, 106\,\mathrm{km/s}) \\ N(\quad 0\,\mathrm{km/s}, \quad 85\,\mathrm{km/s}) \end{pmatrix}. \tag{32}$$

$N(\mu,\sigma)$ denotes a Gaussian distribution with parameters $\mu$, $\sigma$. These velocity vectors were each applied to stars placed at distances $d$ computed from the apparent $V$ magnitude distribution of a sample of 86 HES C stars without significant p.m. (see Fig. 31), and assuming $M_V = +10$ for dwarf carbon stars. This yields $86 \cdot 100 = 8\,600$ simulated stars.

We now define a coordinate system which is aligned with $(u,v,w)$, i.e., $x$ points away from the Galactic center, $y$ into the direction of Galactic rotation, and $z$ perpendicular to the Galactic plane. The vector $\vec{r}$ pointing from the Sun to a star with galactic coordinates $l$, $b$, at distance $d$ is then:

$$\vec{r} = \begin{pmatrix} x \\ y \\ z \end{pmatrix} = d \cdot \begin{pmatrix} -\sin b \\ \cos b \sin l \\ \sin b \end{pmatrix}. \tag{33}$$

After the time $\Delta t$, the star with velocity vector $(u,v,w)$ can be found at position $\vec{r}'$, which is

$$\vec{r}' = \begin{pmatrix} x' \\ y' \\ z' \end{pmatrix} = d \cdot \begin{pmatrix} -\sin b \\ \cos b \sin l \\ \sin b \end{pmatrix} + \Delta t \cdot \begin{pmatrix} u \\ v \\ w \end{pmatrix}. \tag{34}$$

Using the inverse transformations

$$d' \quad = \quad \sqrt{(x')^2 + (y')^2 + (z')^2} \tag{35}$$

$$b' \quad = \quad \arcsin \frac{z'}{d'} \tag{36}$$

$$l' \quad = \quad \arcsin \frac{y'}{d' \cos b'}, \tag{37}$$

we can compute the galactic coordinates $l'$, $b'$ of the star after the time $\Delta t$. Converting $l$, $b$ and $l'$, $b'$ into $\alpha$, $\delta$ and $\alpha'$, $\delta'$ then yields proper motions $\mu_\alpha$, $\mu_\delta$ for each of the 8 600 simulated stars. As starting coordinates $l$, $b$ we take the plate centers of each HES plates, and for $\Delta t$ the epoch difference between DSS I and HES plate, $\Delta t_{\text{HES-DSS I}}$.

Finally, we select the subsample of the 8 600 stars with $\mu_\alpha \cdot \Delta t_{\text{HES-DSS I}} < 4''$, and determine, by multiplication with the selection probability in dependence of $\mu_\delta \Delta t$, the fraction of stars which would be detected in the HES *and* selected by either of the two carbon star selection methods. The result is shown in Fig. 39, and summarized in Tab. 11.

| | Tmatch | C bands |
|---|---|---|
| Selection rate | 36.1 % | 21.4 % |
| Dwarf proof rate | 96.5 % | 61.5 % |

Table 11: Average halo dC selection rates relative to zero p.m., and fraction of provable dwarfs for 329 HES plates.

Another number of interest is the rate of halo dCs which we can *proof* to be dwarfs from their p.m (we shortly call this rate *dwarf proof rate*, d.p.r). We can proof a star to have a luminosity $M_V > M_{V,\max}$, if its transverse velocity $v_{\text{trans}}$ would be larger than the Galactic escape velocity $v_{\text{esc}}$ otherwise, i.e. if

$$\text{p.m.} > \frac{v_{\text{trans}}}{4.74 \cdot 10\,\text{pc}} \cdot 10^{-\frac{m_V - M_{V,\max}}{5}}. \tag{38}$$

For dCs we use $M_{V,\max} = 8$, and we assume $v_{\text{esc}} = 400\,\text{km/s}$. As can be seen in Fig. 39, the d.p.r. is of course much higher for C stars selected by template matching, because with this method stars of higher p.m. can be selected.

Note that for halo dCs in the HES, there is no problem of p.m. *detection* for dCs that can be proven to be dwarfs by their transverse velocity, since it follows from Eq. 38 and the criteria described above that a $V = 16.5$ star must have a p.m. $> 0.17''/\text{yr}$ to be proven to be a dwarf. In Sect. 5.5 we will show that the typical $3\sigma$ uncertainty of the p.m. measurement method we employed is $\sim 0.012''/\text{yr}$ for baselines of $\sim 45$ yrs. So even if only archival images with a 10 years epoch difference were available for comparison with our CCD images, resulting in a $3\sigma$ uncertainty of $\sim 0.054''/\text{yr}$, we could easily detect proper motions $> 0.17''/\text{yr}$.

From the results shown in Tab. 11 and Fig. 38 we can derive correction factors $c$ for the dwarf fractions (in %) we detect in our samples. We define:

$$c = \frac{\text{frac}_{\text{real}}}{\text{frac}_{\text{measured}}}.$$

Let $N_D/N_G$ be the real ratio of dwarfs to giants, and $f_D$, $f_G$ the detection fraction of dwarfs and giants, respectively. Then it can be easily computed that

$$c = \frac{\frac{N_D}{N_G} + \frac{f_G}{f_D}}{\frac{N_D}{N_G} + 1}. \tag{39}$$

According to Green et al. (1992),

$$\frac{N_D}{N_G} = \frac{0.13}{0.87} = 0.15.$$

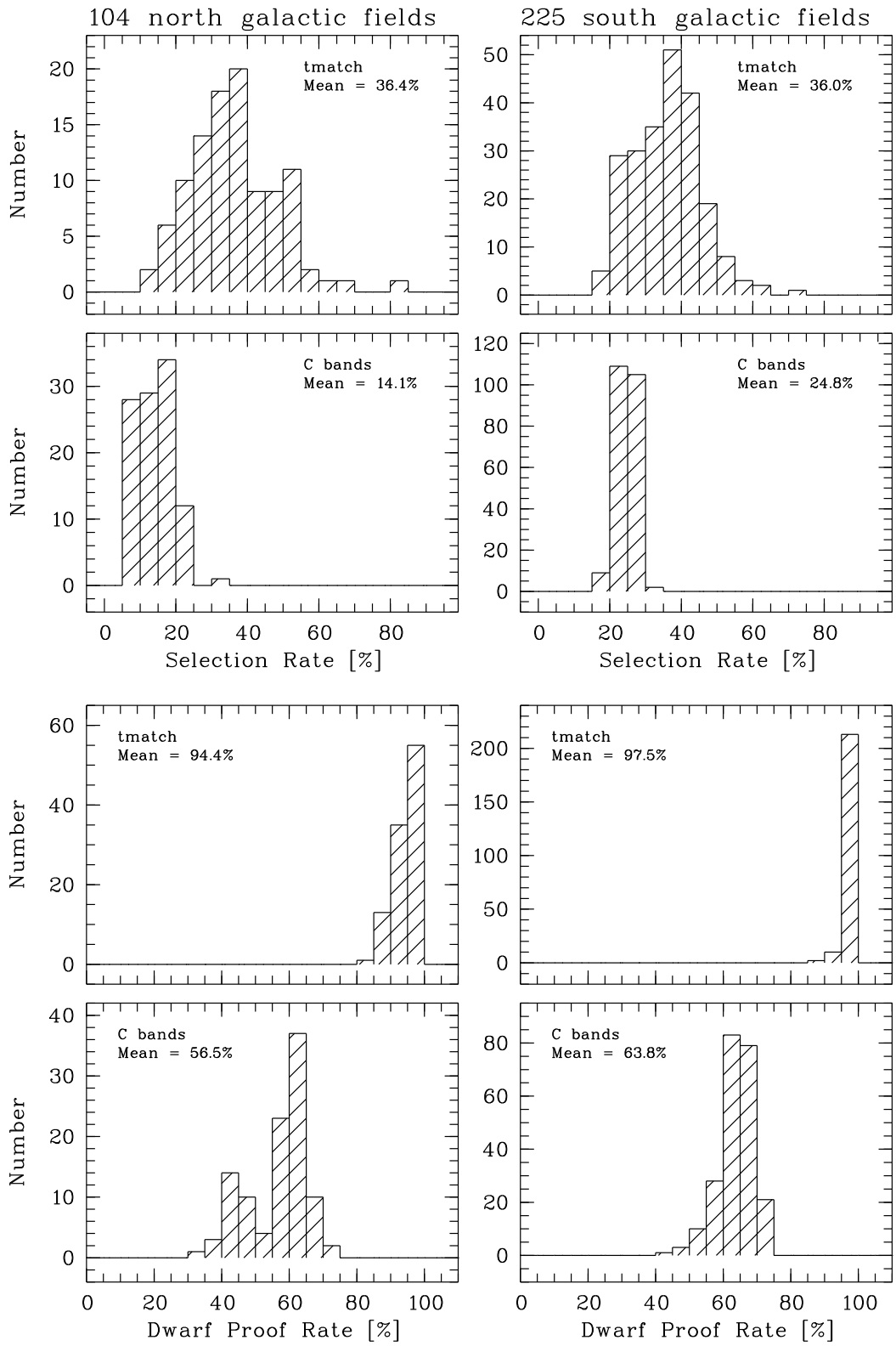


Figure 39: Distribution of plate-wise relative selection probabilities of halo dCs for 329 HES plates.

For the C band index method, we have

$$\frac{f_{G,\text{C band}}}{f_{D,\text{C band}}} = \frac{1.00}{0.214 \cdot 0.615} = 7.60,$$

and for template matching

$$\frac{f_{G,\text{tmatch}}}{f_{D,\text{tmatch}}} = \frac{0.50}{0.361 \cdot 0.965} = 1.44,$$

so that we obtain

$$c_{\text{C band}} = 6.7, \tag{40}$$

and

$$c_{\text{tmatch}} = 1.4. \tag{41}$$

That is, within the C band index selected sample, the dwarf fraction will be 6.7 times lower than it really is, and in the template matching selected sample 1.4 times lower.

Even more interestingly, we will be able to derive the local space density for halo dCs, $N_{\text{dC}}^{\text{halo}}$, by applying the correction factors $f_{D,\text{C band}}$, $f_{D,\text{tmatch}}$ to our flux-limited sample of dCs.

### 5.3.3 Tests with Known C Stars

We also compiled a test sample of known dwarf and giant C stars present on HES plates (see Tab. 12). We took all three dCs in the southern hemisphere listed by Deutsch (1994), i.e. LHS 1075, G77-61, and KA 2. The (possible) dCs of (Warren et al. 1993), having $B_J > 20$, unfortunately are by far too faint to be detectable on HES plates. Cross-identification with the C star lists of Slettebak et al. (1969), Stephenson (1989), Bothun et al. (1991), and Totten & Irwin (1998), yielded 22 stars. Another 6 spectra were produced from slit spectra with the procedures described in Sect. 3.1.

In our test, *all* 22 stars not known as dwarfs have been selected either by their strong $C_2$ bands, or their CN bands, with the band index method. The simulated spectra were also *all* selected either by $C_2$ band indices, or CN indices. For these spectra it was not possible to carry out template matching, because they are noise-free. 13 of the 14 remaining stars below saturation threshold and not known as dwarfs have been selected by template matching. This fraction is much higher than expected from our simulations (50 %). This is probably due to the fact that our test sample is biased towards red objects, with *strong* C bands, so that they are easier to select than the stars in our test sample. Of the three dCs, one (KA 2) has been selected by all methods, one (G77-61) by template matching only, and one (LHS 1075) by neither method.

From these results we conclude that our sample of giant C stars and dwarfs with low p.m. (e.g. dCs belonging to the disk population) is highly complete. From the small number of dCs in our test sample we are not able to draw any definitive conclusions, but our result is consistent with our simulations. Using Poisson statistics, we derive from our test sample that our dC detection rate is $66 \pm 33$ %.

### 5.3.4 Selection Efficiency

Another important criterion for the evaluation of the quality of a selection algorithm is the *selection efficiency*, i.e. the fraction of desired stars in the raw candidate sample. Tab. 13 summarizes the results for both selection methods used.

The C band index method has a much higher selection efficiency than the template matching method. This is because with the latter, a lot of artifacts and noisy spectra are selected. The low fraction of artifacts in the sample selected with the C band method demonstrates that the usage of *pairs*

| Name | HE Name | $B_J$ | $B-V$ | $\mu_\alpha\Delta t$ | $\mu_\delta\Delta t$ | Selected by | | | | |
|---|---|---|---|---|---|---|---|---|---|---|
| | | | | | | $C_2$ | CN | T | All | Source |
| CGCS 39 | HE 0017+0055 | | 1.4 | | | 1 | 1 | – | 1 | S89 |
| SKB 2 | HE 0039−2635 | 13.1 | 1.1 | | | 1 | 1 | – | 1 | SKB69 |
| BEM91 23 | HE 0100−1619 | 15.9 | 1.5 | | | 1 | 0 | 1 | 1 | BEM91 |
| CGCS 177 | HE 0106−2837 | 13.8 | 2.1 | | | 1 | 0 | 1 | 1 | S89 |
| SKB 5 | HE 0111−1346 | 13.3 | 1.4 | | | 1 | 1 | – | 1 | SKB69 |
| 0207-0211 | HE 0207−0211 | 15.5 | 2.2 | 0.0 | 0.0 | 1 | 0 | 1 | 1 | TI98 |
| BEM91 08 | HE 0228−0256 | 16.2 | 2.0 | | | 1 | 0 | 1 | 1 | BEM91 |
| CGCS 525 | HE 0330−2815 | 13.8 | 1.5 | | | 0 | 1 | 0 | 1 | S89 |
| CGCS 935 | HE 0521−3425 | 13.0 | 1.3 | | | 1 | 1 | – | 1 | S89 |
| 0915-0327 | HE 0915−0327 | 14.5 | 2.3 | 0.0 | 0.0 | 1 | 0 | 1 | 1 | TI98 |
| 1019-1136 | HE 1019−1136 | 15.2 | 1.8 | 0.0 | 0.0 | 1 | 0 | 1 | 1 | TI98 |
| CGCS 2954 | HE 1104−0957 | | 1.2 | | | 1 | 1 | – | 1 | S89 |
| KA 2 | HE 1116−1628 | 16.6 | 1.3 | | | 1 | 0 | 1 | 1 | R83 |
| CGCS 3180 | HE 1207−3156 | 12.8 | 1.2 | | | 0 | 1 | – | 1 | S89 |
| CGCS 3274 | HE 1238−0836 | | 1.7 | | | 1 | 1 | – | 1 | S89 |
| 1254-1130 | HE 1254−1130 | 16.1 | 2.2 | 0.0 | 0.0 | 1 | 0 | 1 | 1 | TI98 |
| 1339-0700 | HE 1339−0700 | 15.0 | 1.7 | 0.0 | 0.0 | 1 | 0 | 1 | 1 | TI98 |
| 1442-0058 | HE 1442−0058 | 17.8 | 2.2 | 0.0 | 0.0 | 1 | 0 | 1 | 1 | TI98 |
| CGCS 5435 | HE 2144−1832 | 12.6 | 1.4 | | | 0 | 1 | – | 1 | S89 |
| CGCS 5549 | HE 2200−1652 | 12.3 | 0.9 | | | 1 | 1 | – | 1 | S89 |
| 2213-0017 | HE 2213−0017 | 16.4 | 2.4 | 0.0 | 0.0 | 1 | 0 | 1 | 1 | TI98 |
| 2225-1401 | HE 2225−1401 | 16.5 | 2.9 | 0.0 | 0.0 | 1 | 0 | 1 | 1 | TI98 |
| CLS 50 | | | | 0.0 | 0.0 | 1 | 0 | – | 1 | Simul. |
| CLS 31 | | | | 0.0 | 0.0 | 1 | 1 | – | 1 | Simul. |
| CLS 54 | | | | 0.0 | 0.0 | 1 | 1 | – | 1 | Simul. |
| KA 2 | | | | 0.0 | 0.0 | 1 | 1 | – | 1 | Simul. |
| B1509-0902 | | | | 0.0 | 0.0 | 1 | 1 | – | 1 | Simul. |
| UM 515 | | | | 0.0 | 0.0 | 1 | 0 | – | 1 | Simul. |
| LHS 1075 | HE 0023−1935 | 16.1 | 1.4 | $-0\farcs24$ | $-10\farcs0$ | 0 | 0 | 0 | 0 | D94 |
| KA 2 | HE 1116−1628 | 16.6 | 1.3 | $-0\farcs21$ | $0\farcs24$ | 1 | 0 | 1 | 1 | D94 |
| G77-61 | HE 0330+0148 | 15.0 | 1.4 | $1\farcs9$ | $-7\farcs5$ | 0 | 0 | 1 | 1 | D94 |

Table 12: Test sample of dwarf and giant C stars present on HES plates. Sources: BEM91=Bothun et al. (1991), D94=Deutsch (1994), R83=Ratnatunga (1983), S89=Stephenson (1989), SKB69=Slettebak et al. (1969), TI98=Totten & Irwin (1998). Stars marked with TI98 have been recently reported by Totten et al. (2000) to have no significant p.m. Therefore, we list them with $(\mu_\alpha\Delta t, \mu_\delta\Delta t) = (0,0)$. For some of these stars, we independently obtained a p.m. measurement, too (see Appendix B). Our results agree with those of Totten et al. (2000). Template matching is not carried out for HES spectra above the saturation threshold, because we do not have an estimation of pixel-wise noise for these. KA 2 has not been selected by CN bands, using its real spectrum, but it *has* been selected in the course of our simulations. This is because the $S/N$ at the position of the CN bands is too low in the former spectrum, and effectively infinite in the simulated spectrum.

| | C bands | Tmatch |
|---|---|---|
| Raw candidate reduction factor | 1/2900 | 1/800 |
| C stars | 31.6 % | 2.4 % |
| UNID | 7.0 % | 1.5 % |
| OVL | 29.2 % | 6.6 % |
| ART | 8.7 % | 32.0 % |
| NOIS | 3.8 % | 54.8 % |
| SAT | 15.6 % | 0.0 % |

Table 13: Selection efficiency for C stars in the HES, for both selection methods used. UNID=*probable* C stars with weak C bands, OVL=overlapping spectra, ART=artifacts, NOIS=very noisy spectra, SAT=saturated spectra. The raw candidate reduction factor is the factor by which the selection algorithms reduce the *total* set of HES spectra. For example, the C band index method extracts 1 199 candidates from 3 437 630 spectra present on 329 HES plates.

of $C_2$ bands and CN bands indeed very reliably excludes artifacts from selection. On the other hand, with this method more overlapping spectra are selected, because the band indices can be easily confused by them. The fraction of saturated spectra is zero for the template matching method, because sources above the saturation threshold are excluded from template matching. This is because the template matching method needs an estimate of the pixel-wise noise, and our noise estimation is not valid for saturated spectra.

## 5.4 The Surface Density of C Stars

In an effective area of $\sim 6\,400\,\mathrm{deg}^2$ (329 of 380 the HES plates), we have isolated a total of 351 C stars, selected by either the C band index or the template matching method. In 225 fields, located at $20^h30 <$R.A.$< 06^h30$ ("south Galactic fields"), we find 0.037 FHLC stars deg$^{-2}$. This is almost twice what has been reported by Green et al. (1994) from their own CCD survey and the sum of FHLC stars selected from photographic objective prism surveys then available. Moreover, the CCD survey limit of Green et al. (1994) was $V = 18$, which is also a typical brightness limit for the relevant objective prism surveys, whereas the HES survey limit is $V \simeq 16.5$ (see Fig. 31). Interestingly, the surface density of FHLC stars in 104 fields located at $09^h00 <$R.A.$< 15^h20$ ("north Galactic fields") is almost a factor 3 higher than in the south Galactic fields: In the former we find 0.099 FHLC stars deg$^{-2}$.

## 5.5 Astrometry

To measure the p.m.s of our carbon stars, we obtained $V$ images for 92 FHLC stars at the European Southern Observatory, La Silla, Chile on April 26–28, 1999, using the Wide Field Imager attached to the ESO/MPI 2.2 m telescope.

We compared the CCD positions of our carbon stars with positions from archival plate material. The USNO-A2.0 catalog (Monet et al. 1998), derived from re-scanned Palomar Observatory Sky Survey I (POSS I) plates, provides the earliest epochs; typically in the 1950s. However, POSS I plates are only available at $\delta > -25^\circ$. Additionally, we extracted DSS I and DSS II image data from the ST ScI data archive. When available, the original POSS I images were also retrieved.

Subimages of $8' \times 8'$ size with our targets in the center were extracted from our CCD frames. In these images, we selected 20–60 sufficiently bright, isolated reference stars by hand. These were then used for alignment of the reference coordinate system (provided by the archival data) with the target image. For most of our images it was possible to do carry out three alignments: (1) DSS I/POSS I image to the CCD image, (2) USNO-A2.0 catalog to the DSS II image, and (3) USNO-A2.0 catalog to the CCD image. Since the USNO-A2.0 catalog was generated from POSS I plates, neither of the alignment pairs is independent of the others.

After rejection of reference objects with significant p.m. or measurement errors, the alignment usually employs 15–50 stars, depending on the field density, and deepness of the exposure obtained. The transferred solution is a simple linear solution (sufficient for the small fields used for this purpose) derived with a least-squares fit using procedures from the IDL *Astronomy User's Library* (Landsman 1993) and written in IDL by E.W. Deutsch (University of Washington). The uncertainty in the transfer is typically $\sim 0''.05$. The shift in position of the target star is recorded for each of the three comparisons described above, along with a $1\sigma$ uncertainty estimated from the residuals of the fit. We report here only the results from the transfer of the USNO-A2.0 catalog positions to the CCD images, but the other solutions are examined to verify these results.

Candidates have been selected to have a significant p.m. measurement if (a) their p.m. is higher than $3\times$ the $1\sigma$ uncertainty estimate from the USNO-A2.0 to CCD comparison, (b) the results from the other comparisons are consistent, and (c) no nearby companions are present which might cause significant centroiding errors. Tab. 14 shows coordinates of the 5 stars out of our sample of 92 for which we measure a significant p.m. Astrometry results for these stars are given in Tab. 15. Stars without significant p.m. are listed in Tab. 25 and 26, in Appendix B.

| # | Name | $\alpha(2000.0)$ | $\delta(2000.0)$ | Epoch |
|---|---|---|---|---|
| 1 | HE 0930−0018 | 09 33 24.7 | −00 31 46 | 1983.4 |
| 2 | HE 0945−0813 | 09 48 18.7 | −08 27 40 | 1983.4 |
| 3 | HE 1428−1950 | 14 30 59.4 | −20 03 42 | 1976.5 |
| 4 | HE 1429−0551 | 14 32 31.3 | −06 05 00 | 1983.3 |
| 5 | HE 1524−0210 | 15 26 56.9 | −02 20 45 | 1979.5 |

Table 14: Coordinates of 5 HES carbon stars with significant p.m.

In addition to our targets, we carried out a new proper motion measurement for KA 2 (Ratnatunga 1983; Green et al. 1992; Deutsch 1994), which was rediscovered in our survey. A comparison of our result with previous measurements is given in Tab. 16. Our values are in good agreement with those of Ratnatunga (1983) and Deutsch (1994). Green et al. (1992) reported a marginal detection of a p.m. for this object in the same order of magnitude as that of Ratnatunga (1983), but with opposite sign in $\mu_\alpha$, which disagrees with our result.

From our p.m. measurements, Eq. (38), and photometry presented in Tab. 17 we conclude that one star (HE 0930−0018) out of the 5 new HES carbon stars for which we measure a significant p.m. is likely to be a dwarf, and another (HE 0945−0813) is possibly a subgiant.

## 5.6 Discussion and Conclusions

In an effective area of $\sim 6\,400\,\mathrm{deg}^2$ (329 of 380 the HES plates), we have isolated a total of 351 C stars. Our efforts have thus already increased the number of known FHLC stars by a factor of nearly five.

| # | Name | $\mu_\alpha$ | $\mu_\delta$ | $\mu$ | Baseline |
|---|---|---|---|---|---|
| | | $\sigma_{\mu_\alpha}$ | $\sigma_{\mu_\delta}$ | $\sigma_\mu$ | |
| 1 | HE 0930-0018 | −0.051 | 0.034 | 0.061 | 1955.0–1999.3 |
| | | 0.005 | 0.004 | 0.005 | |
| 2 | HE 0945-0813 | 0.004 | 0.012 | 0.013 | 1953.0–1999.3 |
| | | 0.004 | 0.004 | 0.004 | |
| 3 | HE 1428-1950 | 0.014 | 0.006 | 0.015 | 1953.0–1999.3 |
| | | 0.003 | 0.003 | 0.003 | |
| 4 | HE 1429-0551 | −0.005 | −0.014 | 0.015 | 1954.4–1999.3 |
| | | 0.003 | 0.003 | 0.003 | |
| 5 | HE 1524-0210 | 0.003 | −0.012 | 0.012 | 1953.0–1999.3 |
| | | 0.004 | 0.003 | 0.003 | |

Table 15: Proper motions for 5 HES carbon stars with significant p.m. For each object we list in the first row the proper motion in arcseconds per year, and in the second row $1\sigma$ errors.

| Reference | $\mu_\alpha$ | $\mu_\delta$ | $\sigma_{\mu_\alpha}$ | $\sigma_{\mu_\delta}$ |
|---|---|---|---|---|
| This work | −0.020 | 0.027 | 0.003 | 0.004 |
| Deutsch (1994) | −0.026 | 0.031 | 0.003 | 0.003 |
| Ratnatunga (1983) | −0.026 | 0.024 | 0.003 | 0.003 |

Table 16: Comparison of astrometry results for KA 2. Proper motions and errors are given in arcseconds per year.

| # | Name | $B_J$ | $(B-V)^*_{\rm HES}$ | $(B-V)_{\rm CCD}$ | $B^{**}_{\rm HES}$ | $B_{\rm CCD}$ | $V_{\rm HES}$ | $V_{\rm CCD}$ |
|---|---|---|---|---|---|---|---|---|
| 1 | HE 0930-0018 | 15.7 | 1.4 | – | 16.1 | – | **14.7** | – |
| 2 | HE 0945-0813 | 16.2 | 1.2 | – | 16.5 | – | **15.3** | – |
| 3 | HE 1428-1950 | 12.8 | 1.2 | 1.15 | 13.1 | 13.15 | 11.9 | **12.00** |
| 4 | HE 1429-0551 | 13.4 | 1.4 | 1.28 | 13.8 | 13.94 | 12.4 | **12.67** |
| 5 | HE 1524-0210 | 14.5 | 1.5 | 1.56 | 14.9 | 15.70 | 13.4 | **14.14** |
| | KA 2 | 16.6 | 1.3 | – | 16.9 | – | **15.6** | – |

* From calibration of `dx_hpp2` (see Tab. 6).

** Following Hewett et al. (1995), we use $B = B_J + 0.28 \cdot (B-V)$.

Table 17: Photometry for the 5 carbon stars with significant p.m. $B_J$ is measured on HES plates and is accurate to $\pm 0.2$ mag. Adopted $V$ magnitudes are written in bold.

| # | Name | $\mu^*$ | $M^{**}_{V,\min}$ | Dwarf ($M_V = 10$) | | | Giant ($M_V = -1$) | |
|---|---|---|---|---|---|---|---|---|
| | | | | $d$ | $\pi$ | $v^{***}_{\rm trans}$ | $d$ | $v^{***}_{\rm trans}$ |
| 1 | HE 0930-0018 | $0\farcs061$ | 4.0 | 87 pc | $0\farcs011$ | 25 km/s | 14 000 pc | 4 000 km/s |
| 2 | HE 0945-0813 | $0\farcs013$ | 1.2 | 110 pc | $0\farcs0091$ | 6.8 km/s | 18 000 pc | 1 100 km/s |
| 3 | HE 1428-1950 | $0\farcs014$ | $-2.0$ | 25 pc | $0\farcs040$ | 1.7 km/s | 4 000 pc | 260 km/s |
| 4 | HE 1429-0551 | $0\farcs015$ | $-1.4$ | 35 pc | $0\farcs029$ | 2.5 km/s | 5 400 pc | 390 km/s |
| 5 | HE 1524-0210 | $0\farcs013$ | $-0.7$ | 66 pc | $0\farcs015$ | 4.1 km/s | 11 000 pc | 660 km/s |
| | KA 2 | $0\farcs033$ | 8.6 | 130 pc | $0\farcs0076$ | 21 km/s | 21 000 pc | 3 300 km/s |

* $\mu = \sqrt{\mu_\alpha^2 \cos^2\delta + \mu_\delta^2}$.

** Assuming $v_{\rm trans} < 400$ km/s ($\sim$ Galactic escape velocity).

*** $v_{\rm trans}\,[\text{km/s}] = 4.74 \cdot \mu[''/\text{yr}] \cdot d[\text{pc}]$.

Table 18: Distances and transverse velocities for 5 HES carbon stars with significant p.m., for the assumptions that they are dwarfs or giants.

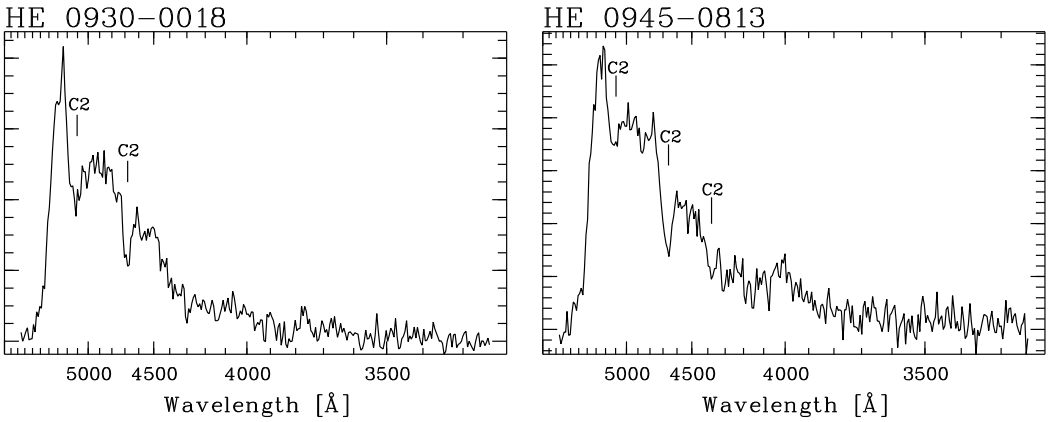


Figure 40: Objective prism spectra of the carbon stars HE 0930−0018 and HE 0945−0813, discovered in the HES. According to our proper motion measurement, HE 0930−0018 is likely to be a dwarf, and HE 0945−0813 is possibly a subgiant. Abscissae are densities in arbitrary units.

The surface density of FHLC stars found in the HES indicates that previous surveys suffer from severe incompleteness. For instance, at a survey limit $\sim 1.5^m$ *brighter* than the CCD survey of Green et al. (1992), we find a factor of $\sim 2$ higher surface density of FHLC stars in 225 southern galactic latitude fields (0.037 deg$^{-2}$), and a factor of $\sim 5$ higher surface density in 104 northern Galactic fields (0.099 deg$^{-2}$). This corresponds to $\sim 16\times$ and $\sim 40\times$ higher space densities of C stars, respectively. The south Galactic fields are located at higher galactic latitude on average ($|b| = 60^\circ$ compared to $|b| = 45^\circ$), but the mean plate limits of the corresponding HES plates do not differ significantly, so that a scale height effect might be present.

Our results indicate that previous FHLC selection procedures have been less sensitive to the strength or variety of $C_2$ or CN molecular bands. Automatic selection techniques may be superior to visible inspection of objective-prism spectra with binocular microscopes, as done e.g. in the survey of Sanduleak & Pesch (1988). Photometric surveys for C stars have generally selected red objects only, which preferentially selects mostly the much less common high latitude AGB stars.

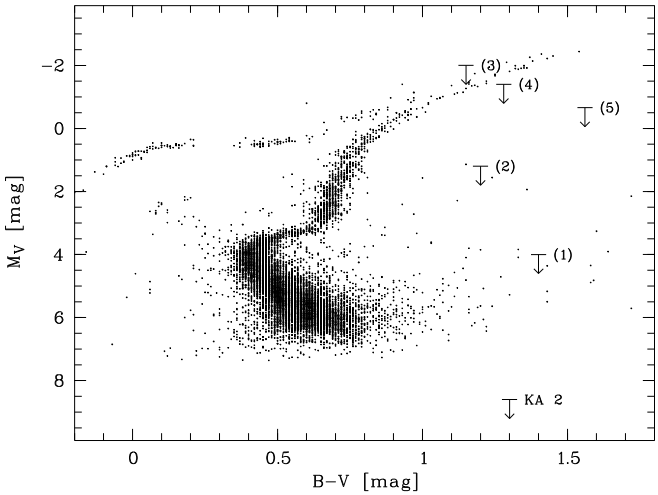


Figure 41: Upper limits for $M_V$ of 5 HES carbon stars with significant p.m., and KA 2, for orientation shown together with the HR diagram of the old (18.7 Gyr), metal-poor ([Fe/H] = −1.66) globular cluster M 3 = NGC 5272 (Buonanno et al. 1994). $M_V$ has been computed from the data of Buonanno et al. (1994) by assuming $m_v - M_V = 15.10$ (Reid 1999).

Due to an average epoch difference of 13.5 years between DSS I and HES plates, we expect to detect and select only $\sim 40\,\%$ of the dCs that we could detect and select if direct plates had been taken simultaneously with the HES plates. However, our extensive simulations yielded correction factors for the dwarf fraction in our sample (Eqs. 40 and 41).

Our corrected dwarf fractions predict $92 \cdot 0.13/6.7 = 1.8$ provable dwarfs to be present in our sample of 92 FHLC stars observed in April '99 with the ESO 2.2 m. This is consistent with the one *provable* dwarf we found, when applying the criterion $M_V > 8$ and assuming $v_{\rm esc} = 400$ km/s. This dC is the previously known star KA 2.

Using again the dwarf fraction obtained by Green et al. (1992), we can estimate how many provable dCs we expect to find in the HES. We selected a total of 347 C stars with the C band index method. Assuming a selection efficiency for giants of 100 % and using the numbers in Tab. 11, we derive that this sample should consist of 336 giants and 11 dwarfs, of which we can proof 7 to be dwarfs by their p.m. On this basis we predict that another 39 dwarfs should be out there in space which we miss by the C band index method. Of the total of 50 dwarfs, we can select 18 by template matching, according to our simulations, and 17 of them we can proof to be dwarfs. Half of the dCs found with the C band index method are expected to be found by template matching as well, so that we predict to find a total of $17 + 7 \cdot 0.5 \simeq 21$ provable dwarfs. This would *triple* the sample of known dCs.

## 5.7 Outlook

With HE 0930−0018 we found a star which is likely to be a new dwarf. If any of the remaining four C stars for which we measure a significant p.m. is a dwarf, it would have a parallax which is measurable from ground-based observatories (see Tab. 18). Therefore, and to get a definitive answer for HE 0930−0018, we are seeking all 5 stars to be observed in a long-term parallax program. Alternatively, parallaxes could be easily measured by the upcoming new generation of astrometry satellites, like FAME and SIM.

HE 0930−0018 is also scheduled to be observed at high resolution in the commissioning phase

of the High Dispersion Spectrograph (HDS) at the Subaru telescope for an abundance analysis, and to derive stellar parameters spectroscopically.

CCD images of another 109 C stars and 10 control objects have been obtained with the ESO 2.2 m telescope in November 1999. These are currently being analyzed. 8 hours of observing time in period 65 (April–October 2000) has been granted to our project by ESO, so that another $\sim 80$ targets will soon be observed.

We plan to obtain *JHK* photometry for all new dCs we discover in the HES, and also for as many stars without p.m. as possible. Should dCs be confirmed to be distinguishable from giants by *JHK* colors (as suggested by the results of Green et al. 1992), we would be able to construct a luminosity criterion. This is very important for all kinematic studies using carbon stars, since a contamination by a significant number of dwarfs (*at least* 13 % according to Green et al. 1992) would bias the results considerably. Moreover, being able to identify all giants means that we are also able to identify all *disk* dCs in our sample, which are less easily found by means of p.m. This would allow us to estimate the local space density of disk dCs, $N_{\rm dC}^{\rm disk}$, and test the model for the space density of dCs suggested by de Kool & Green (1995). Their model predicts a strong metallicity dependence of the fraction of binaries in which the secondary becomes a dC. Taking the $\sim 500$ times higher local space density of disk stars into account (Bahcall & Soneira 1984), de Kool & Green (1995) predict that $N_{\rm dC}^{\rm disk}$ is 2.5–5 times higher than $N_{\rm dC}^{\rm halo}$.

### Acknowledgements

I thank my fellow “dwarf hunters”, P. Green and E. Deutsch, for a very productive and joyful collaboration, and many discussions. From Paul I learned much about the scientific background of current C star research. He also provided me with a list of known C stars, and with slit spectra for some of them. Eric provided his neat IDL programs, and processed *more* than half of our 92 CCD images with them when we were visiting Paul at the Harvard-Smithsonian Center for Astrophysics (CfA), because he is much faster at it than I am!

Paragraphs 3–5 of Sect. 5.5 have been originally written by Eric for an article which is in preparation; I just added a few further explanations and remarks. The same holds for paragraphs 3–5 of the introduction, which have been written by Paul.

I acknowledge the hospitality shown to me at CfA, where part of the work described in this section was carried out.

## References

Bahcall, J. N. & Soneira, R. M. (1984), ‘Comparisons of a standard galaxy model with stellar observations in five fields’, *ApJS* **55**, 67–99.

Bothun, G., Elias, J. H., MacAlpine, G., Matthews, K., Mould, J. R., Neugebauer, G. & Reid, I. N. (1991), ‘Carbon stars at high Galactic latitude’, *AJ* **101**, 2220–2228.

Brewer, J. P., Richer, H. B. & Crabtree, D. R. (1996), ‘Late-type stars in M31. II. C-, S-, and M-star spectra’, *AJ* **112**, 491–508.

Buonanno, R., Corsi, C. E., Buzzoni, A., Cacciari, C., Ferraro, F. R. & Pecci, F. F. (1994), ‘The stellar population of the globular cluster M 3. I. Photographic photometry of 10 000 stars’, *A&A* **290**, 64.

Castleman, K. R. (1979), *Digital Image Processing*, Prentice Hall, Englewood Cliffs.

Christlieb, N. (1995), Automatische Klassifikation von digitalisierten Objektivprismen-Platten, Diplomarbeit, Universität Hamburg.

Dahn, C. C., Liebert, J., Kron, R. G., Spinrad, H. & Hintzen, P. M. (1977), 'G77-61 – A dwarf carbon star', *ApJ* **216**, 757–766.

de Kool, M. & Green, P. J. (1995), 'A model for the space density of dwarf carbon stars', *ApJ* **449**, 236–245.

Dearborn, D. S. P., Liebert, J., Aaronson, M., Dahn, C. C., Harrington, R., Mould, J. & Greenstein, J. L. (1986), 'On the nature of the dwarf carbon star G77-61', *ApJ* **300**, 314–324.

Deutsch, E. W. (1994), 'Positions and Proper Motions of Dwarf Carbon Stars', *PASP* **106**, 1134–1137.

Green, P. J. & Margon, B. (1994), 'Constraints on the origin of dwarf carbon stars', *ApJ* **423**, 723–732.

Green, P. J., Margon, B. & Anderson, S. F. (1992), 'Carbon star luminosity indicators', *ApJ* **400**, 659–664.

Green, P. J., Margon, B. & MacConnell, D. J. (1991), 'Three newly recognized dwarf carbon stars', *ApJ* **380**, L31–L34.

Green, P. J., Margon, B., Anderson, S. F. & Cook, K. H. (1994), 'A CCD survey for faint high-latitude carbon stars', *ApJ* **434**, 319–329.

Heber, U., Bade, N., Jordan, S. & Voges, W. (1993), 'PG 0824+289: a dwarf carbon star with a visible white dwarf companion', *A&A* **267**, L31–L34.

Hewett, P. C., Foltz, C. B. & Chaffee, F. H. (1995), 'The Large, Bright QSO Survey. VI. Quasar Catalog and survey parameters', *AJ* **109**, 1498–1521.

Landsman, W. B. (1993), The IDL Astronomy User's Library, *in* R. J. Hanisch, R. J. V. Bissenden & J. Barnes, eds, 'ADASS II', Vol. 52 of *ASP Conf. Ser.*, pp. 246–248.

Liebert, J., Schmidt, G. D., Lesser, M., Stepanian, J. A., Lipovetsky, V. A., Chaffe, F. H., Foltz, C. B. & Bergeron, P. (1994), 'Discovery of a dwarf carbon star with a white dwarf companion and of a highly magnetic degenerate star', *ApJ* **421**, 733–737.

MacAlpine, G. M. & Lewis, D. W. (1978), 'Curtis Schmidt-thin prism survey for extragalactic emission-line objects. University of Michigan List IV.', *ApJS* **36**, 587–593.

Margon, B., Anderson, S. F., Deutsch, E. W. & Harris, H. C. (1999), Faint Carbon Stars Discovered by the Sloan Digital Sky Survey, *in* 'AAS Meeting 195', p. #80.06.

McCook, G. P. & Sion, E. M. (1999), 'A catalog of spectroscopically identified white dwarfs', *ApJS* **121**, 1–130.

Monet, D. G., Bird, A. & Canzian, B. (1998), USNO-A2.0: A catalog of astrometric standards, Technical report, U.S. Naval Observatory.

Morrison, H. L., Mateo, M., Olszewski, E. W., Harding, P., Dohm-Palmer, R. C., Freeman, K. C., Norris, J. E. & Morita, M. (2000), 'Mapping the Galactic Halo I. The "Spaghetti" Survey', *ApJ* **?**, ? in press (astro-ph/0001492).

Mould, J. R., Schneider, D. P., Gordon, G. A., Aaronson, M. & Liebert, J. W. (1985), 'The velocity dispersion of carbon stars at the north Galactic pole', *PASP* **97**, 130–137.

Norris, J. (1986), 'Population studies. II – Kinematics as a function of abundance and galactocentric position for [Fe/H]$\leq -0.6$', *ApJS* **61**, 667–698.

Ratnatunga, K. U. (1983), Outer regions of the Galactic halo, PhD thesis, Australian National University, Canberra.

Reid, I. N. (1999), 'The HR Diagram and the Galactic Distance Scale After Hipparcos', *ARAA* **37**, 191–237.

Sanduleak, N. & Pesch, P. (1988), 'The Case low-dispersion northern sky survey. VII. Late-type stars', *ApJS* **66**, 387–390.

Slettebak, A., Keenan, P. C. & Brundage, R. K. (1969), 'Carbon stars in a south galactic pole region', *AJ* **74**, 373–374.

Stephenson, C. B. (1989), 'A General Catalog of Cool Galactic Carbon Stars, 2nd Edition', *Publ. W.&S. Obs*.

Totten, E. J. & Irwin, M. J. (1998), 'The APM survey for cool carbon stars in the Galactic halo. I', *MNRAS* **294**, 1–27.

Totten, E. J., Irwin, M. J. & Whitelock, P. A. (2000), 'The APM survey for cool carbon stars in the Galactic halo. II. The search for dwarf carbon stars', *MNRAS* **000**, 000–000. in press (astro-ph/0001113).

Warren, S. J., Irwin, M. J., Evans, D. W., Liebert, J. W., Osmer, P. S. & Hewett, P. C. (1993), 'More dwarf carbon stars', *MNRAS* **261**, 185–189.